Interpretation of the vacuum ultraviolet photoabsorption spectrum of iodobenzene by *ab initio* computations

Michael H. Palmer,[1] Trevor Ridley,[1] Søren Vrønning Hoffmann,[2,] Nykola C. Jones,[2] Marcello Coreno,[3] Monica de Simone,[4] Cesare Grazioli,[4,5] Malgorzata Biczysko,[6,7] Alberto Baiardi,[7] and Paulo Limão-Vieira[8]

[1]*School of Chemistry, University of Edinburgh, Joseph Black Building, David Brewster Road, Edinburgh EH9 3FJ, Scotland, United Kingdom*

[2]*Department of Physics and Astronomy, ISA, Aarhus University, Ny Munkegade 120,DK-8000 Aarhus C, Denmark*

[3]*CNR-ISM, Montelibretti, c/o Laboratorio Elettra, Trieste, Italy*

[4]*CNR-IOM Laboratorio TASC, Trieste, Italy*

[5]*Department of Chemical and Pharmaceutical Sciences, University of Trieste, Trieste, Italy*

[6]*National Research Council ICCOM-CNR, UOS di Pisa, Via G. Moruzzi 1, I-56124 Pisa, Italy*

[7]*Scuola Normale Superiore, Piazza Cavalieri 7, 56126 Pisa, Italy*

[8]*Laboratório de Colisões Atómicas e Moleculares, CEFITEC, Departamento de Física, Faculdade de Ciências e Tecnologia, Universidade Nova de Lisboa, 2829-516 Caparica, Portugal*

Abstract

Identification of many Rydberg states in iodobenzene, especially from the first and fourth ionization energies (IE_1 and IE_4, X^2B_1 and C^2B_1), has become possible using a new ultraviolet (UV) and vacuum-ultraviolet (VUV) absorption spectrum, in the region 29 000-87 000 cm^{-1} (3.60-10.79 eV), measured at room temperature with synchrotron radiation. A few Rydberg states based on IE_2 (A^2A_2) were found, but those based on IE_3

(B^2B_2) are undetectable. The almost complete absence of observable Rydberg states relating to IE_2 and IE_3 (A^2A_2 and B^2B_2, respectively) is attributed to them being coupled to the near-continuum, high-energy region of Rydberg series converging on IE_1. Theoretical studies of the UV and VUV spectra used both time-dependent density functional (TDDFT) and multi-reference multi-root doubles and singles-configuration interaction methods. The theoretical adiabatic excitation energies, and their corresponding vibrational profiles, gave a satisfactory interpretation of the experimental results. The calculations indicate that the UV onset contains both 1^1B_1 and 1^1B_2 states with very low oscillator strength, while the 2^1B_1 state was found to lie under the lowest $\pi\pi^*$ 1^1A_1 state. All three of these $^1B_1$ and $^1B_2$ states are excitations into low-lying σ^* orbitals. The strongest VUV band near 7 eV contains two very strong $\pi\pi^*$ valence states, together with other weak contributors. The lowest Rydberg $4b_16s$ state (3^1B_1) is very evident as a sharp multiplet near 6 eV; its position and vibrational structure are well reproduced by the TDDFT results

I. INTRODUCTION

In this paper, we present new high-resolution, synchrotron-excited 1-photon, vacuum ultraviolet (VUV) absorption spectra, and in the accompanying paper (AP),[1] photoelectron spectra (PES) of iodobenzene (*PhI*), both at room temperature. In several respects, the spectra of *PhI* are the most complex of the monohalobenzenes (C_6H_5I, C_6H_5Br, C_6H_5Cl, and C_6H_5F, "the series," *PhX*) and are difficult to interpret in isolation. We will be presenting similar studies of the lower members of the series later, where we will also present (2 + 1) and (3 + 1) resonance enhanced multiphoton ionization (REMPI) spectra of jet-cooled samples. The present analyses of the VUV spectrum (and PES) are supported by *ab initio* configuration interaction (CI) and time dependent density functional (TDDFT) calculations of vertical and adiabatic ionization (and excitation) energies and vibrationally resolved spectra.

The most intense bands in the absorption spectrum are valence in nature. The three main bands in the ultraviolet (UV) spectrum of *PhI* have maxima near 4.88, 5.49, and 5.99 eV. These well-known[2–5] bands are present in solution and hence are valence rather than Rydberg states. They also closely resemble the principal singlet transitions in benzene (4.86, 6.20, and 6.97 eV). However, the situation is more complex, since alkyl iodides show absorption near 260 nm (4.77 eV) in the UV region,[3–5] attributed to $\sigma^* \leftarrow$ n valence transitions. This additional interaction with the *PhI* ring and σ- and π-MOs (a_1 and b_1, respectively) is exemplified by the electron density contours shown in Fig. 1(a) for the four highest MOs; and Fig. 1(b) for the LUMOs involved in the low energy excitations. In order to correlate transitions across the series of *PhX*, it is convenient to use valence shell numbering of MOs, and these are indicated in Fig. 1. The orbital energies (eV) are as follows: occupied $2b_1$(–9.81), $6b_2$(–8.91), $1a_2$(–8.73), and HOMO $3b_1$(–7.98); virtual orbitals: $7a_1^*$(–0.14), $8a_1^*$(0.28), $4b_1^*$(0.32), and $2a_2^*$(0.41).

The first VUV (4.59 to 11.27 eV) study of the absorption spectrum was unanalyzed,[2] but Kimura and Nagakura[6] fitted the 4.3–7.55 eV region to six Gaussian bands; their theoretical analysis, using only π-MOs on C and I atoms, was limited to $\pi\pi^*$ and charge-

transfer (C-T) states, as discussed by Robin.[5]

No Rydberg states of *PhI* have been observed previously in either VUV absorption[2–6] or earlier REMPI studies,[7,8] but we observe numerous Rydberg states in the current spectrum and we use the new analysis of the PES[1] as an aid to assigning these states. PES are important for identification of Rydberg states in the VUV absorption spectrum since the potentials experienced in the ionic (PES) and Rydberg state (VUV) formation, particularly for high-*n* states, are similar and this leads to similar vibrational profiles in the two types of spectra.[9–15] Therefore, in the analysis of the absorption spectra, we use the vibronic structure observed in the PES[1] as a fingerprint to identify the ionic core of the observed Rydberg state or series.

The current VUV spectrum goes up to approximately 11 eV; therefore, the first four ionic state band systems for *PhI* are relevant. We propose in AP[1] that three of them are coupled and consequently in the VUV spectra the Rydberg series converging on these ionization limits are also coupled making assignment of the spectra more difficult. Despite these factors, we have been able to identify, with reasonable certainty, the ionic core of most of the observed Rydberg states. In addition, characteristic quantum defects are used to further assign a considerable number and variety (s,p,d,f) of Rydberg states.

Our VUV study concentrates on static spectral behaviour, rather than dynamic aspects, so that the known homolytic photochemical decomposition of *PhI* at several wavelengths,[16,17] and references therein, is peripheral to the present study. It is sufficient to note that no evidence of the known photolysis products, which include molecular iodine and biphenyl (*Ph-Ph*) formation were observed in our spectral studies. The colour formation of I_2 is a particularly strong guide concerning potential photolysis. The very low experimental C–I bond dissociation energy of *PhI* ($D_0 = 2.900$ eV)[16] is clearly responsible for many of these reactions.

The theoretical aspect of this study includes determination of adiabatic and valence excited state excitation energies for several low-lying singlet states. The Franck-Condon (FC) spectral profiles[18–21] were determined using MCSCF and TDDFT methods.[22–24] The

corresponding vertical study, which enables many more states to be studied over a much wider energy range, uses multi-reference multi-root CI methods (MRD-CI).[25–27] In some parts of the study, the basis sets included *ab initio* relativistic effective potentials which include spin–orbit operators.[28–31] Variations in molecular structure with electronic state are shown in the supplementary material.[32]

In the VUV and PES discussion below, our units are electron volts (eV) for wide energy range UV + VUV spectra. However, since we are interested in the vibrational structure of the bands, this makes cm^{-1} a more suitable energy unit for the Rydberg state study.

II. EXPERIMENTAL AND COMPUTATIONAL PROCEDURES

A. Experimental VUV absorption

The VUV absorption spectrum was measured on the ASTRID2 storage ring at Aarhus University, Denmark, using the AU-UV beam line. The AU-UV beam line was originally commissioned on ASTRID in 2000; it was known then as the UV1 beam line and is described in detail in Eden *et al*.[33] In order to utilize the new 3rd generation light source, ASTRID2, the beam line has undergone significant changes. The geometry of the old beam line, with a source to first mirror distance of 1700 mm, was such that it could not be directly attached to the new storage ring, as a radiation wall had to be accommodated. Therefore, a pair of 1:1 focussing pre-optics mirrors was installed to image the source to an intermediate focus (*IF*), which acts as a source for the existing beam line without further alteration.

A toroidal mirror (TM2) focuses the beam from the *IF* onto the entrance slit (ENS) (Fig. 2), which is typically set to 100 μm for photoabsorption measurements. The light then passes to a toroidal grating. There are two gratings available, a high energy grating (HEG) with a line density of 2000 lines/mm covering 100-350 nm (12.40 to 3.54 eV) and a low energy grating (LEG) with a line density of 1000 lines/mm covering 160-700 nm (7.75 to 1.77 eV). The light exits the monochromator via a moveable slit (EXS), also set to 100 μm, and passes through a LiF window which separates the ultra-high vacuum of the beam

line from the end station experiment. The resolution of the monochromator using the HEG, the primary grating used for high resolution photoabsorption measurements, has been measured and found to be 0.08 nm over the operational range of the grating (≡13 cm^{-1} at 250 nm and 50 cm^{-1} at 125 nm), close to the calculated value of 0.07 nm.[33]

The apparatus used for measurement of photoabsorption spectra has also undergone several alterations since that described in Eden *et al*.[33] The new cell (see Fig. 3), which allows moderate (up to 80 °C) heating of a sample during measurement, has a path length of 15.5 cm and is fitted with a heated 1 Torr Baratron capacitance manometer (Setra model 774). The light exits the cell through a MgF_2 window, which sets the lower limit of detectable light to 115 nm. A small gap between the photo-multiplier tube (PMT) detector and the absorption cell is evacuated using a scroll pump for measurements below 200 nm. Above 200 nm, air is allowed into this gap to let oxygen absorb higher orders of light (at half the chosen wavelength) which may be passing through the cell. In this way, photoabsorption measurements can be performed with spectrally pure radiation from 115 nm to 340 nm, ensuring artefact-free spectra.

Absolute photoabsorption cross-sections (σ) are obtained using the Beer-Lambert law

$$I_t = I_0 \exp(-n\sigma l),$$

where I_t and I_0 are the detector signal transmitted through a gas and for an evacuated cell, respectively, l is the cell path length (15.5 cm) and n is the molecular number density (derived from the pressure measurement). ASTRID2 is operated in a so-called top-up mode, keeping the stored electron beam current (and thus the intensity for a given wavelength) quasi constant by adding small amounts of current to ASTRID2 to make up for the constant beam decay. The beam current thus varies about 3%-5% during a scan, and this is taken into account by recording and normalizing to an accurately determined beam current.

In order to accurately determine cross-sections, the VUV spectrum was recorded in small (5 nm or 10 nm) sections, with at least 1 nm overlap to the adjoining sections. For each

section of the spectrum, a scan with no gas in the cell was first recorded (I_0). Then, an appropriate pressure of sample for each range was selected so that the incoming light was attenuated by 40%-50%, which is low enough to prevent line saturation effects and two scans of the sample in a static gas cell recorded (I_t). The cell was then evacuated and a second scan of the empty cell recorded. The final cross-sections were then calculated using all four of these scans. A single scan typically took 4–5 min; consistency between the two I_t scans recorded and the good overlap of the sections of the spectrum indicated no degradation of the sample in the cell during the timescale of the measurements.

The photoabsorption spectrum for *PhI* was measured in the energy range from 3.594 eV (345 nm, 28 988 cm^{-1}) to 10.781 eV (115 nm, 86 954 cm^{-1}) using data points separated by 0.05 nm (4-40 cm^{-1}) and is shown in Fig. 4.

The samples of *PhI* (CAS Registry Number 591-50-4) were obtained from Sigma-Aldrich and used without further purification apart from repeated freeze-pump-thaw cycles in order to remove air.

B. Experimental PES

A new PES measured on the gas phase beam line of the Elettra synchrotron, described in AP[1] is used here. The high-resolution spectrum, recorded using 30 eV photons, covers the range 8.167–24.625 eV; the low energy region up to 11.5 eV shown in Fig. 5 was recorded in steps of 0.001 eV. The measured IEs (Table I) crucial to the current Rydberg state identification involving bands 1 to 3 (Fig. 5) show the ionization processes IE , (IE + IE), and IE , respectively, which are also indicated on the VUV absorption spectrum (Fig. 4).

C. Computational methods

Adiabatic excitation energies (AEEs) of several singlet and ionic states were obtained using either the TDDFT method[22–24] or state-averaged (SA) MCSCF methods implemented in GAUSSIAN-09.[34,35] Vibrational FC profiles[18–21] were generated from both TDDFT and unrestricted Hartree-Fock (UHF) (ionic) wave-functions within the

Adiabatic Hessian approximation (FCAH) also taking into account temperature effects. Only a few AEEs were determined, since root swapping in the energy sequence, where many states have rather similar structures, prevented the success of the computational focus on some states. Thus, vertical excitation energies (VEE) for valence and Rydberg states, determined by a MRD-CI[25-27],as implemented in GAMESS-UK,[36] were also utilized; this method is fully described in our previous studies.[13–15]

In this paper, theoretical oscillator strengths (f(r)), derived from the CI wave-functions, are compared with absorption band intensities. Wide differences in f(r) occur between valence and Rydberg states, generally enabling differentiation between the types of excitation. Typical values are 10^{-1}–10^{-2} and 10^{-2}–10^{-6}, respectively, but unexpectedly, in the present study, some valence states (e.g., both 1^1B_1 and 1^1B_2) have very low f(r). The second moments of the charge distribution (SMCD, $\langle x^2 \rangle$, $\langle y^2 \rangle$, and $\langle z^2 \rangle$) give additional information both in relation to valence states, which have similar values for SMCD to the ground state, and also concerning the directionality of Rydberg p-, d-, and f-states, where selected directions of the SMCD are large; this procedure was described previously.[13–15]

In all the CI methods, the 29 core orbitals ($15a_1 + 5b_1 + 7b_2 + 2a_2$) are frozen in occupancy and density; the full valence shell occupied orbitals ($8a_1 + 3b_1 + 6b_2 + 1a_2$) were included in the CI, together with up to 120 virtual MOs (VMOs) in the MRD-CI study. Valence shell numbering is used to enable comparisons with the lower *PhX*. These C_{2v} molecules all lie in the yz-plane, where the z-axis lies along the C_2 axis.

D. Basis sets

The *ab initio* C- and H-atom bases were chosen to be compatible in style with the more limited I-atom basis sets.[37,38] Overall, the Sadlej p-VTZ (I) basis sets[39] in combination with the TZVP (C,H) basis[40] were widely used; these gave I[11s8p6d2f], C[5s3p2d], H[3s2p] contracted functions. Unexpectedly, in several equilibrium structure searches for the ionic states, these bases at both the MCSCF and UHF theoretical levels led to saddle points rather than full minima. The effective core potential (ECP) quasi-relativistic basis

sets including CRENBL[41] and SDD[30,31] gave genuine minima in both the UHF and TDDFT methods. Indeed, CRENBL generated VEE nearly identical to the all-electron basis set using MRD-CI and structures close to the MCSCF methods. For our Rydberg state studies, the CRENBL basis wasextended by sets of s-, p-, d-, and f-functions. By incorporating separate s-, p-, d-, and f-enhancements, the ECP enabled the energy determination of higher Rydberg states to be performed more economically.

III. RESULTS AND DISCUSSION

A. Overall aspects of the UV + VUV absorption spectrum of *PhI* and its theoretical interpretation

Our experimental UV + VUV spectrum (Fig. 4) also shows our calculated valence shell VEEs and their oscillator strengths, which includes excitations from both π- and σ-MOs; the full list of VEE state energies, oscillator strengths, and SMCD is presented in the supplementary material.[32] The SMCD can be used to demonstrate the directionality of the Rydberg states and hence their symmetry.[13–15]

Expansions of short energy ranges of the UV + VUV spectrum are exhibited below; the dominant three regions of the spectrum are near 5.5, 6.5, and 7 eV; each of these ranges show high f(r) valence states. The most intense individual band lies between 7 and 7.5 eV and can be correlated with two calculated ππ* electronic states, of $^1A_1$ ($1a_2 2a_2^*$) and $^1B_2$ ($2b_1 2a_2^* - 1a_2 4b_1^*$) symmetries, together with other weaker states. The AEEs of the valence states that could be calculated, together with the corresponding VEEs, are shown in Table II.

B. Valence states

1. The 3.7-6.0 eV region

The absorption spectrum in the region 3.7-6.0 eV consists of two broad bands with some vibrational structure superimposed on them, as shown in Figs. 6 and 7, and these have

been commonly labelled as bands A and B. The spectroscopy and dynamics of these bands have been the focus of many studies, of which that of Sage *et al*.[16] which includes a thorough, critical review of previous studies[42–46] is the most recent and comprehensive. Experimentally, Sage *et al*.[16] studied photodissociation following 1-photon absorption, using REMPI excitation of the atomic iodine that was generated. The kinetic energies of the atoms were measured using velocity mapped ion imaging (VMI) detection. The experimental data were supported by *ab initio* calculations on the excited states that included spin-orbit coupling (SOC). The most important conclusion from the experimental results was that the photodissociation process over the whole region was almost entirely due to the initial 1-photon absorption via parallel transitions, i.e., into A_1 states. On the basis of the *ab initio* calculations, band A was assigned to the first excited SOC A_1 state, $2A_1$, that was predominantly made up from the spin-orbit free (SOF) $^3B_1$ $\pi\sigma^*$ state. Band B was assigned to the SOC $5A_1$ state which was almost entirely made up from the SOF 1^1A_1 $\pi\pi^*$ state, in line with most previous studies.

We have calculated the geometry of the SOF 1^1A_1 state and simulated its absorption spectrum. The AEE (and vibrational complexity exhibited) for the 1^1A_1 $\pi\pi^*$ state is very dependent on the basis set within the TDDFT procedure; using the ECP containing the CRENBL basis, the 1^1A_1 state has the AEE 5.658 eV (f(r) = 0.2089), and hence is very close to the observed band origin of 5.42 eV. However, the FC profile is much simpler than that obtained with the much larger all-electron study using the Sadlej + aug-cc-pVTZ basis sets, and a stick spectrum of the intensities obtained from this latter calculation is shown in Fig. 7. The AEE is significantly low by this process, and the calculated band has been shifted by +0.408 eV to give a close overlay with the experimental band structure. The calculated vibrational frequencies are in excellent agreement with those observed and the intensities are also acceptable. All of the vibrational structure is assigned to a_1 modes, notably ν_5, ν_8, ν_9, ν_{10}, and ν_{11}, with frequencies of 1581, 984, 970, 612, and 266 cm^{-1}, respectively. The fundamental bands are labelled in Fig. 7, with the remainder of the bands being due to overtones and combinations of those modes as shown in Table III.

A ladder generated from the vibrational modes and frequencies observed for band B is shown above the experimental band A absorption shown in Fig. 6, where the origin is aligned with the first identifiable band in the spectrum at 4.6 eV. The accuracy with which the legs of the ladder point to the partially resolved structure strongly suggest that the same modes are active in bands A and B.

As described above, this band is assigned to the SOC $2A_1$ state. Since we do not include SOC in our calculations, we cannot produce a simulation for this band. However, it is clear that neither of our calculated FC Factor (FCF) for the two SOF singlet states in this region, 1^1B_1 and 1^1B_2, shown in Fig. 6, have the required vibrational profiles to give rise to the majority of the observed spectrum. The calculated oscillator strength of the latter is much greater than the former and hence it may make a minor contribution to the total absorption. Indeed, Sage *et al*.[16] observed very weak signals due to the initial 1-photon absorption via a perpendicular transition, i.e., into a B_1 or B_2 state in the long wavelength region of band A.

The nature of the potential energy surfaces of the SOC $2A_1$ and $5A_1$ states and how these account for the observed photodissociation dynamics has been discussed in detail by Sage *et al*.[16] In brief, the $2A_1$ state that gives rise to band A is dissociative in the C–I coordinate at the equilibrium ring geometry and the slow rise in the continuum absorption starting at 3.78 eV reflects the increasing FC overlap along this coordinate. Our calculations confirm that the SOF $^3B_1$ state, that is the chief component of the $2A_1$ state after SOC, is dissociative. Beginning at ~4.6 eV, there are absorptions into coordinates that are not dissociative, e.g., the ring breathing modes,ν_8 and ν_9, as shown in Fig. 6. The molecule then survives for several vibration periods before emerging along the dissociative coordinate. In contrast, the $5A_1$ state that gives rise to band B does not have a dissociative C–I coordinate at the equilibrium ring geometry and the largest FC overlaps are with bound levels. As above, the molecule survives for several vibration periods before dissociation which in this case involves transfer to dissociative surfaces of lower-lying A_1 states.

We have carried out detailed calculations on the SOF 1^1B_1, 1^1B_2, and 2^1B_1 states in addition to the 1^1A_1 state. Using the TDDFT method, the calculated energies of the 0-0 transitions of the 1^1B_1 and 1^1B_2 states are 4.416 and 4.664 eV, respectively, with the maximum of the former at 4.938 eV. The FC calculated vibrational intervals (Table III) show that 1^1B_1 is dominated by a single progression of ν_{11} (152 cm^{-1}); 1^1B_2 shows a series of fundamentals, in which the frequencies of the strongest vibrations are 265, 641, 978, and 1459 cm^{-1}. The very weak 1^1B_1 state, shown in Fig. 6 with scaled intensity, exhibits a slow rise in strength at the onset and high quanta ($v \sim 20$) at the maximum; it is dominated by the $4b_1a_1^*$ configuration. The 1^1B_2 state contains both the $6b_2a_1^*$ and $2a_2b_1^*$ configurations. The vibrational energy distributions for these two states are totally different, but in both these states, a low-lying σ^* MO ($11a_1^*$ in the valence shell numbering) is present.

The 2^1B_1 state lies in the region of band B but has a very low intensity relative to that of the overlapping 1^1A_1 state. It has very similar vibrational structure to the 1^1B_1 state, also being dominated by a single progression in ν_{11} with a frequency of 138 cm^{-1}, slightly lower than in the 1^1B_1 state (152 cm^{-1}), and reaching a maximum at $v \sim 50$. The similarity between the 1^1B_1 and 2^1B_1 states is enhanced by the leading configurations being excitation from $3b_1$ and $2b_1$ into the same a_1^* MO, although the 2^1B_1 state has a significant contribution from the $8b_22a_2^*$ configuration (c.f. Fig. 1).

Instead of evenly balanced combinations of $b_1b_1^* \pm a_2a_2^*$ ($^1A_1$) and $b_1a_2^* \pm a_2b_1^*$ ($^1B_2$), the *PhI* electronic structure leads to the dominance of each of these configurations over four $\pi\pi^*$ states. Thus, the lowest $^1A_1$ state is dominated by $3b_14b_1^*$ with lower densities of $3b_15b_1^*$ and $1a_22a_2^*$. Several of our higher $^1A_1$ states have a similar FC profile to that in Fig. 7, including those at 7.367, 8.087, 8.818, and 8.870 eV.

2. The 6.0 to 6.9 eV region

The lowest Rydberg state ($3b_13s$ or $3b_16s$, using either the valence shell or all-electron numbering) is immediately observable (Fig. 8). We have determined the equilibrium

structure of this state by utilizing a combination of valence + CRENBL and Rydberg state functions. In general, it is difficult or impossible to obtain an equilibrium structure for a diffuse state such as this, especially in polyatomic molecules; this difficulty arises from the proximity of various valence states in the same energy region and state "swapping" during the optimization process. At equilibrium, the Rydberg state shows the C–I bond (2.060 Å) is slightly shortened from the X^1A_1 ground state (2.127 Å). The complexity of the Rydberg band is apparent from the tail of the progressions; the vibrational envelope is dominated by several quanta of the low-frequency mode ν_{11} but other fundamentals including ν_7 and ν_6 with various combination bands also occur. The remainder of the band between 6.2 and 6.9 eV (see Fig. 4) contains a group of both singlet and triplet valence states; discussion of this region is deferred to the supplementary material.[32]

The results showed that in this region, the energy differences between planar ring structures and distortion to C_S symmetry are small, and distortion may also occur for several bands. This leads to additional complexity, since forbidden $^1A_2$ states become allowed in C_S symmetry.

3. Bands above 7.0 eV

The strongly absorbing region from 7.0 to 7.5 eV of the VUV spectrum is relatively featureless. Vertical excitation studies suggest that several electronic states lie under this band, where the $^1A_1$ states have high oscillator strength. The most intense excited state (AEE 7.322 eV with an f(r) of 0.973) is a symmetric combination of ($3b_1b_1^* + 1a_2a_2^*$) states. Although it is a relatively high excitation, the equilibrium structure is close to the C_{2v} ground state, with a C–I bond length of 2.094 Å. The $^1B_2$ state at 7.622 eV with an f(r) of 0.581 is largely $2b_1a_2^*$, with a C–I bond length of 2.100 Å, and all CC and CH bonds lengthened and shortened, respectively, with respect to the equilibrium structure. Above this energy, the equilibrium structures and frequencies for only a few excited states were obtained. A $\pi\pi^*$ state (f(r) 0.196) at 8.054 eV is dominated by complex mixtures of $b_1b_1^* \pm b_2b_2^* \pm a_2a_2^*$ configurations, but still has a structure close to equilibrium with a C–I

bond of 2.086 Å and CC bonds of 1.395 ± 0.010 Å. In contrast, the 8.818 eV $^1B_2$ state (f(r) 0.118) shows significant structural changes with a C–I bond of 2.188 Å and shortening of the C_2–C_3/C_5–C_6 bonds.

C. Rydberg states observed in the VUV absorption spectrum

1. Overall aspects

We have used a procedure similar to our previous studies[13–15] to enable distinction between the valence and Rydberg types of spectra. In order to help identify features in the VUV spectrum as Rydberg states, an underlying broad structure made up of several Gaussian bands was "subtracted" from the original spectrum.[13–15] The result is shown in Fig. 9(a), where assignments of s-, p-, d-, and f-series converging on the first IE are also shown; such an analysis would be much more problematic without the "subtraction" procedure. This can be seen most clearly in part of the high-energy region of the spectrum shown in Fig. 9(b). The top (black) trace shows the raw spectrum while the lower red trace shows the spectrum which is obtained by subtracting a single Gaussian peak of which the region shown forms part of the rising edge. An amplification of the "background subtracted" spectrum which reveals sharp Rydberg peaks is shown in the upper red trace. The justification of this process is immediately apparent when comparing the narrow (i.e., sharp) vibrational structure of the PES bands responsible for the Rydberg states, with the much broader valence band structure.

The Rydberg states were identified by comparison of the local vibrational structure with individual PES band envelopes and the transition energies of the electronic origins of the states are shown in Table IV. Since the vibrational levels in the Rydberg states are their principal characteristic, it is convenient to use cm^{-1} as the energy unit. Also shown in Table IV are the effective quantum numbers, n^* values, of the origins, calculated using the conventional Rydberg formula and the appropriate IE (see Table I), which are used to assign the nl values of the states. We emphasize that the assignments of the Rydberg series are based on comparisons of the n^* values with those of other polyatomic

molecules, e.g., methyl iodide and furan,[13–15,47,48] and not on the current *ab initio* calculations.

Most of these Rydberg identifications are based on the first ionization energy (IE_1, X^2B_1). Of these, only a single Rydberg series was identified from the complete sets of two (p-type) and four (d-type) Rydberg series that are 1-photon allowed, but two of the five allowed f-type series were observed. In addition, several Rydberg states based on IE_4 (C^2B_1) were identified but very few based on IE_2 and IE_3. In AP[1], we propose that the A^2A_2 and B^2B_2 states of the ion are coupled to the high-energy region of the X^2B_1 state and we will discuss below the consequences of this on the absorption spectrum.

The SOC that affects the low-lying valence states must also impinge on the Rydberg states to some extent. However, we assume that the states that are observable in the VUV absorption spectrum are all predominantly singlet in character and we will omit the "singlet" label in the following Rydberg state discussions.

2. Series converging on IE_1

We have identified the origins of ~20 Rydberg states converging on IE_1. The assignments are illustrated in Figs. 10 and 11 in which the ladders indicate v = 0, 1, 2, and 3 of ν_{11} the lowest frequency totally symmetric vibration, built on the electronic origin indicated. Above $n = 6$, the nd-, nf-, and $(n + 1)$s-series merge and are arbitrarily labelled nd in Table IV.

The assignment of the sharp bands with an origin at 48 742 cm^{-1} ($n^* = 2.24$) as the 3s state is unambiguous (see above). However, the ν_{11} progression is slightly different from that of the PES of the ground state of the ion, and of most Rydberg states converging on it, in two respects: (i) the vibrational spacing of 310 cm^{-1} is significantly greater than the commonly observed value of ~285 cm^{-1} (the calculated value for the 3s state is 291 cm^{-1} and (ii) the relative intensities of the bands in the ν_{11} progression are also different. Both observations indicate an interaction with a second B_1 electronic state and our calculations show that a B_1 valence makes a major contribution to the absorption in this region (see

Fig. S3 of supplementary material[32]).

Only one very weak 3p state and one medium intensity 3d state is assigned. The three most intense bands in the region of the 4p states with an onset at 61 460 cm^{-1} are separated by ~220 cm^{-1}, i.e., not consistent with a Rydberg state based on the ground state of the ion. Therefore, these are assigned as the 3s Rydberg state based on IE_4, the C^2B_1 state of the ion, at 85 035 cm^{-1}, yielding $n^* = 2.15$. The 4p state is assigned to three weak bands separated by ~280 cm^{-1} and starting at 61 858 cm^{-1}. There are more bands observed around 64 000 cm^{-1} than can be explained by an extrapolation of what is seen in the 3d/4s region. Consequently, we assign two 4f, as well as one 4d and one 5s state as shown in Fig. 11(a). The remainder of the bands up to IE_1 is assigned to higher members of these series which merge as n increases as shown in Fig. 11(b).

3. Series converging on IE_4

The Rydberg series converging on IE_4 are indicated in Fig. 12 and the transition energies of the electronic origins are presented in Table IV. Transitions to only five IE_4 states are 1-photon allowed in the 3d/4s region, whereas at least eight peaks can be observed in the spectrum and therefore some of these must be due to Rydberg states with IE_2/IE_3 ionic cores.

If the interpretation of the PES is correct, the fingerprint of IE_3 is defined by two bands of similar intensity separated by ~800 cm^{-1} but no pairs of bands are observed with this separation in this region. Therefore, in this energy region, we assign five bands to the origins of n = 5-9 members of the np-series converging on IE_2. In addition, we assign three [4]3d and one [4]4s states in this region, where [4] denotes a state with an IE_4 ionic core. The remainder of the bands up to IE_4 is assigned to higher members of these series which merge as n increases as shown in Fig. 12.

The PES of the C^2B_1 state of the ion shows a progression of partially resolved bands separated by ~210 cm^{-1}. It appears that these bands in the Rydberg states converging on IE_4 only become sharp enough to be resolved for $n \geq 8$ as shown in Fig. 12. The widths of

the bands in the [4]3d region are ~400 cm^{-1} compared with ~150 cm^{-1} for those in the n = 10 region. The threshold for the change in the widths is around IE_3 as shown in Fig. 12.

4. Series converging on IE_2 and IE_3

Only one Rydberg series converging on either IE_2 or IE_3 has been identified which we believe is due to their large bandwidths. In AP[1], we show that in order to simulate the observed PES, increasingly large bandwidths are required for the X^2B_1, A^2A_2, and B^2B_2 state bands. Narrow vibrational structure re-emerges in the C^2B_1 state band.

Kwon *et al*.[49] also observed a very broad origin band of the B^2B_2 state of *PhI* in their mass analyzed threshold ionization (MATI) spectrum and equated it to a lifetime of <100 fs, where the lifetime refers to the time that the ion remains in its initially populated level before internal conversion (IC) to a dense manifold of levels of a lower state. Bâldea *et al*.[50,51] also cited fs IC, in this case to the X^2B_1 state, to explain the broad A^2A_2 bands observed in the PES of *PhF*. In *PhI*, we believe that the B^2B_2 state undergoes IC to the A^2A_2 state which in turn undergoes IC to the X^2B_1 state. We note that the broadening cannot be attributed to predissociation, since the dissociation energy of the *PhI* cation ($C_6H_5^+$ + I) is much higher (11.2(1) eV; 90 334 cm^{-1}).[52]

The bandwidths observed in the PES have an impact on the Rydberg state peaks observed in the VUV absorption spectrum since the potentials experienced in the ionic and Rydberg state are similar.[9–15] First, the total intensity of any band is proportional to its area and hence for two bands with equal intensity, the peak height of a broadened band will be much smaller than one which is not broadened and consequently will be difficult to identify in regions where peaks with both widths occur. Second, overlap of these broadened bands will lead a near-continuum absorption leading to additional difficulty in observing them in the spectrum. Both factors can explain why only one Rydberg series converging on IE_2 and none converging on IE_3 are identified.

The Rydberg series converging on IE_4 must be superimposed on and therefore may couple with these pseudocontinua of Rydberg series converging on IE_2 and IE_3. The widths of the

[4]*n*l bands in the [4]3d region in the absorption spectrum are around 400 cm^{-1}, the same as those of the [2]*n*p- series in the same region and hence are consistent with all of the states being coupled. At energies above IE_3, any coupling will decrease and the Rydberg states converging on IE_4 will become relatively sharp as shown in Fig. 12. While no states with an IE_3 ionic core are identified in the VUV spectrum of *PhI*, we will show in subsequent papers that Rydberg series converging on IE_3 are prominent in the equivalent spectra of *PhBr* and *PhCl* thus presenting a major contrast.

Furthermore, we have recently obtained an enhanced PES for the perfluoro-compound C_6F_5I which has made practical a re-analysis of its VUV spectral data. In the PES, the IE_3 and IE_4 bands are equally prominent and several Rydberg series converging on both IEs can be identified in the absorption spectrum.

IV. CONCLUSIONS

The interpretation of the experimental UV + VUV spectrum of *PhI* in the 4-11 eV range is by far the most detailed yet reported. The vibrational structure in the spectra has been analyzed using a combination of adiabatic TDDFT and vertical (MRDCI) sets of calculations; the band origins between theory and experiment require only small adjustments of the energy scale (generally less than 0.4 eV) to superimpose the FC vibrational structure from the calculations onto the main experimental bands. Much of the structure of the UV and low energy VUV bands is explicable in terms of the FC analyses presented.

Our simulation of the vibrational profile of the $\pi\pi^*$ $^1A_1$ state including hot bands accurately reproduces that of the observed absorption near 5.4 eV, band B, confirming that this state is the main contributor to the band, as expected from its large oscillator strength. In contrast, our simulations of the profiles of the two valence states, 1^1B_1 and 1^1B_2, both involving excitation from MO $3b_1$ and $8b_2$ into the lowest σ^* (a_1 symmetry) MO do not reproduce the contour of the absorption near 4.8 eV, band A. These two states, although both are formally allowed, have particularly low oscillator strengths. Both

findings are consistent with the proposal that SOC has to be taken into account to explain the absorption spectrum and photodissociation dynamics in this region.[16]

The strong band which stands out in the VUV spectrum between 5.9 and 6.9 eV is preceded by the lowest Rydberg state. Several states were identified by TDDFT energy minimization and FC analysis in this energy range, including a pair of $\pi\pi^*$ states with underlying weak vibrational structure. The strongest individual band in the spectrum shown in Fig. 4, lying between 7 and 7.5 eV, is again dominated by $\pi\pi^*$ states.

The present UV + VUV spectral profile shows a number of similarities to that of C_6F_5I,[53] with the characteristics of slow onset (above 4 eV), main $\pi\pi^*$ band near 5 eV, and major maxima above 7 eV; however, in the latter case, the presence of the F-atoms leads to significant shift of the $^1A_1$ and $^1B_2$ components of the 7 eV band of the *PhI* molecule, by the "perfluoro effect."[54]

We have made extensive use of FC vibrational profiles observed in the PES to identify the main vibrational progressions occurring in the VUV absorption spectra. A considerable number of Rydberg states were identified at higher energy in the spectrum and, using the raw data from AP[1] on ionic states for *PhI*, the Rydberg states were categorized. The use of the vibrational profiles from the PES is critical to these identifications, owing to the density of states apparent in the VUV spectrum, and in that respect, the TDDFT method proved valuable.

A considerable number of Rydberg series converging on the X^2B_1 and C^2B_1 states have been identified but only one converging on the A^2A state and none on the B^2B state, the four lowest ionic states for *PhI*. We believe that this is due to the B^2B_2 ionic state undergoing IC to the A^2A_2 state which in turn undergoes IC to the near-continuum, high-energy region of the X^2B_1 state. Consequently, the [2]*n*l and [3]*n*l series converging on the A^2A and B^2B limits will be similarly broadened and hence not resolvable in the absorption spectrum. A similarity with the VUV spectrum of C_6F_5I was noted,[53] but our recent redetermination of the PES for C_6F_5I has led us to conclude that further study of the VUV spectrum would be essential to complete a correlation.

ACKNOWLEDGMENTS

The authors wish to acknowledge: (a) beam time allocated at the ASTRID2 synchrotron at ISA Aarhus University, Denmark; (b) C. Puglia (Uppsala University, Sweden) and the Carl Tygger Foundation for making available the VG-Scienta SES-200 photoelectron analyser at the Gas Phase beamline, Elettra, Italy; (c) support of the NSCCS (National super-computing service in the UK to M.H.P.); (d) the financial support provided by the European Commission through the Access to Research Infrastructure action of the Improving Human Potential Programme, FP6- Transnational Access Programme IA-SFS:R113-CT-2004- 50600; (e) M.B. acknowledges support by the Italian MIUR (under the Project No. PON01-01078/8) and PRIN 2011 DEMOCRITOS; (f) P.L.V. acknowledges partial funding from the research Grant Nos. PEst-OE/FIS/UI0068/2014 and PTDC/FIS-ATO/1832/2012 through the Portuguese Foundation for Science and Technology, FCT-MEC as well as support from the British Council for Portuguese-English joint collaboration. The research leading to these results has received funding from the European Community's Seventh Framework Programme (No. FP7/2007-2013) CALIPSO under Grant Agreement No. 312284. We all thank Professor Vincenzo Barone and Dr. Julien Bloino for helpful discussions and Professor N. J. Mason for access to an earlier recording of the VUV spectrum of *PhI*.

References

[1]M. H. Palmer, T. Ridley, S. Vrønning Hoffmann, N. C. Jones, M. Coreno, M. de Simone, C. Grazioli, M. Biczysko, and A. Baiardi, J. Chem. Phys. 142, 134301 (2015).

[2]W. C. Price and A. D. Walsh, Proc. R. Soc. London, Ser. A 191, 22 (1947).

[3]K. Kimura and S. Nagakura, Spectrochim. Acta 17, 166 (1961).

[4]H. H. Jaffe and M. Orchin, *Theory and Applications of Ultraviolet Spectroscopy* (Wiley, Chichester, 1962).

[5]M. B. Robin, *Higher Excited States of Polyatomic Molecules* (Academic Press, New York, 1974), Vol. 2.

[6]K. Kimura and S. Nagakura, Mol. Phys. 9, 117 (1965).

[7]T. D. Scarborough, J. Strohaber, D. B. Foote, C. J. McAcy, and C. J. G. J. Uiterwaal, Phys. Chem. Chem. Phys. 13, 13783 (2011).

[8]X.-P. Zhang, Z.-R. Wei, Y. Tang, T.-J. Chao, B. Zhang, and K.-C. Lin, ChemPhysChem. 9, 1130 (2008).[9]M. S. Child, *Theory of Molecular Rydberg States* (Cambridge University Press, Cambridge, 2011).

[10]T. F. Gallagher, *Rydberg Atoms* (Cambridge University Press, Cambridge, 1994).

[11]R. S. Mulliken, J. Am. Chem. Soc. 86, 3183 (1964). J. Chem. Phys. **142**, 134302 (2015)

[12]R. S. Mulliken, J. Am. Chem. Soc. 88, 1849 (1966).[13]M. H. Palmer, P. J. Camp, S. V. Hoffmann, N. C. Jones, A. R. Head, and D. L. Lichtenberger, J. Chem. Phys. 136, 094310 (2012).

[14]M. H. Palmer, S. V. Hoffmann, N. C. Jones, A. R. Head, and D. L. Lichtenberger, J. Chem. Phys. 134, 084309 (2011).

[15]M. H. Palmer, S. V. Hoffmann, N. C. Jones, E. R. Smith, and D. L. Lichtenberger, J. Chem. Phys. 138, 214317 (2013).

[16]A. G. Sage, T. A. A. Oliver, D. Murdock, M. B. Crow, G. A. D. Ritchie, J. N. Harvey,

and M. N. R. Ashfold, Phys. Chem. Chem. Phys. 13, 8075 (2011).

[17]D. Murdock, M. B. Crow, G. A. D. Ritchie, and M. N. R. Ashfold, J. Chem. Phys. 136, 124313 (2012).

[18]V. Barone, J. Bloino, and M. Biczysko, GAUSSIAN 09, Revision A.02, Gaussian, Inc., 2009.

[19]J. Bloino, M. Biczysko, O. Crescenzi, and V. Barone, J. Chem. Phys. 128, 244105 (2008).

[20]V. Barone, J. Bloino, M. Biczysko, and F. Santoro, J. Chem. Theory Comput. 5, 540 (2009).

[21]V. Barone, J. Chem. Phys. 122, 014108 (2005).

[22]R. E. Stratmann, G. E. Scuseria, and M. J. Frisch, Chem. Phys. Lett. 257, 213 (1996).

[23]M. E. Casida, C. Jamorski, K. C. Casida, and D. R. Salahub, J. Chem. Phys. 108, 4439 (1998).

[24]R. Bauernschmitt and R. Ahlrichs, Chem. Phys. Lett. 256, 454 (1996).

[25]R. J. Buenker, in *Current Aspects of Quantum Chemistry*, edited by R. Carbo (Elsevier, New York, 1982), p. 17.

[26]R. J. Buenker and R. A. Phillips, Theochem 24, 291 (1985).

[27]R. J. Buenker and S. Krebs, in *Recent Advances in Multireference Methods*, edited by K. Hirao (World Scientific, Singapore, 1999), p. 1.

[28]P. J. Hay and W. R. Wadt, J. Chem. Phys. 82, 299 (1985).

[29]W. J. Stevens, M. Krauss, H. Basch, and P. G. Jasien, Can. J. Chem. 70, 612 (1992).

[30]G. Igel-Mann, H. Stoll, and H. Preuss, Mol. Phys. 65, 1321 (1988).[31]D. Andrae, U. Haussermann, M. Dolg, H. Stoll, and H. Preuss, Theor. Chim.Acta 77, 123 (1990).

[32]See supplementary material at http://dx.doi.org/10.1063/1.4916121 for the following: singlet state equilibrium structures; further details of the MRD- CI vertical excitation to singlet states; logarithmic plot of the calculated oscillator strengths for valence states; and

the interpretation of the 6 to 6.9 eV region of the VUV spectrum.

[33]S. Eden, P. Limao-Vieira, S. V. Hoffmann, and N. J. Mason, Chem. Phys. 323, 313 (2006).

[34]M. J. Frisch, G. W. Trucks, H. B. Schlegel, G. E. Scuseria, M. A. Robb, J. R. Cheeseman, G. Scalmani, V. Barone, B. Mennucci, G. A. Petersson, H. Nakatsuji, M. Caricato, X. Li, H. P. Hratchian, A. F. Izmaylov, J. Bloino, G. Zheng, J. L. Sonnenberg, M. Hada, M. Ehara, K. Toyota, R. Fukuda, J. Hasegawa, M. Ishida, T. Nakajima, Y. Honda, O. Kitao, H. Nakai, T. Vreven, J. A. Montgomery, Jr., J. E. Peralta, F. Ogliaro, M. Bearpark, J. J. Heyd, E. Brothers, K. N. Kudin, V. N. Staroverov, R. Kobayashi, J. Normand, K. Raghavachari, A. Rendell, J. C. Burant, S. S. Iyengar, J. Tomasi, M. Cossi, N. Rega, J. M. Millam, M. Klene, J. E. Knox, J. B. Cross, V. Bakken, C. Adamo, J. Jaramillo, R. Gomperts, R. E. Stratmann, O. Yazyev, A. J. Austin, R. Cammi, C. Pomelli, J. W. Ochterski, R. L. Martin, K. Morokuma, V. G. Zakrzewski, G. A. Voth, P. Salvador, J. J. Dannenberg, S. Dapprich, A. D. Daniels, Ö. Farkas, J. B. Foresman, J. V. Ortiz, J. Cioslowski, and D. J. Fox, GAUSSIAN 09, Revision D.01, Gaussian Inc., Wallingford CT, 2009.

[35]H.-J. Werner, P. J. Knowles, F. R. Manby, M. Schütz, P. Celani, T. Korona, R. Lindh, A. Mitrushenkov, G. Rauhut, K. R. Shamasundar, T. B. Adler, R. D. Amos, A. Bernhardsson, A. Berning, D. L. Cooper, M. J. O. Deegan, A. J. Dobbyn, F. Eckert, E. Goll, C. Hampel, A. Hesselmann, G. Hetzer, T. Hrenar, G. Jansen, C. Köppl, Y. Liu, A. W. Lloyd, R. A. Mata, A. J. May, S. J. McNicholas, W. Meyer, M. E. Mura, A. Nicklaß, D. P. O'Neill, P. Palmieri, K. Pflüger, R. Pitzer, M. Reiher, T. Shiozaki, H. Stoll, A. J. Stone, R. Tarroni, T. Thorsteinsson, M. Wang, and A. Wolf, MOLPRO, version 2012.1, a package of *ab initio* programs, 2012, see http://www.molpro.net.

[36]M. F. Guest, I. J. Bush, H. J. J. Van Dam, P. Sherwood, J. M. H. Thomas, J. H. Van Lenthe, R. W. A. Havenith, and J. Kendrick, Mol. Phys. 103, 719 (2005).

[37]K. L. Schuchardt, B. T. Didier, T. Elsethagen, L. Sun, V. Gurumoorthi, J. Chase, J. Li, and T. L. Windus, J. Chem. Inf. Model. 47, 1045 (2007).

[38]D. Feller, J. Comput. Chem. 17, 1571 (1996).

[39]A. J. Sadlej, Theor. Chim. Acta 81, 339 (1992).

[40]A. D. McLean and G. S. Chandler, J. Chem. Phys. 72, 5639 (1980). J. Chem. Phys. **142**, 134302 (2015)

[41]L. A. Lajohn, P. A. Christiansen, R. B. Ross, T. Atashroo, and W. C. Ermler, J. Chem. Phys. 87, 2812 (1987).

[42]K. Kavita and P. K. Das, J. Chem. Phys. 117, 2038 (2002).[43]H. J. Hwang, J. Griffiths, and M. A. El-Sayed, Int. J. Mass Spectrom. Ion Processes 131, 265 (1994).[44]P. Y. Cheng, D. Zhong, and A. H. Zewail, Chem. Phys. Lett. 237, 399 (1995).

[45]H. J. Hwang and M. A. El-Sayed, J. Photochem. Photobiol., A 102, 12 (1996).

[46]M. Kadi, J. Davidsson, A. N. Tarnovsky, M. Rasmusson, and E. Akesson, Chem. Phys. Lett. 350, 93 (2001).[47]R. J. Donovan, J. T. Hennessy, K. P. Lawley, and T. Ridley, J. Chem. Phys. 138, 134308 (2013).

[48]T. Ridley, K. P. Lawley, and R. J. Donovan, Phys. Chem. Chem. Phys. 6, 5304 (2004).

[49]C. H. Kwon, H. L. Kim, and M. S. Kim, J. Chem. Phys. 116, 10361 (2002).

[50]I. Bâldea, J. Franz, P. G. Szalay, and H. Köppel, Chem. Phys. 329, 65 (2006).

[51]E. Gindensperger, I. Bâldea, P. G. Szalay, and H. Köppel, Chem. Phys. 338, 207 (2007).

[52]Y. Malinovich and C. Lifshitz, J. Phys. Chem. 90, 2200 (1986).[53]S. Eden, M. J. Hubin-Franskin, J. Delwiche, S. V. Hoffmann, N. J. Mason, and N. C. Jones, Chem. Phys. 359, 111 (2009).[54]C. R. Brundle, N. A. Keubler, and M. B. Robin, J. Am. Chem. Soc. 94, 1466 (1972).

Figure Captions

FIGURE 1 (a), (b) Equal electron density contours and nodal properties. (a) The four highest occupied MOs; when ionized the sequence changes to 3b1 < 1a2 < 6b2 < 2b1; (b) four lowest valence unoccupied (virtual) MOs of *PhI*; in the lowest excited singlet states, the 9a1* MO is occupied.

FIGURE 2 SchematicoverviewoftheAU- UV beam line optics on ASTRID2.

FIGURE 3 Schematic overview of the photoabsorption apparatus. The main body of the cell and the sample can be heated, while keeping the detector and pumps at room temperature. The Baratron is separately heated to 123 °C to avoid molecular condensation.

FIGURE 4 The experimental UV plus VUV absorption spectrum of *PhI*, (black) with superimposed all-electron MRD-CI vertical energies and oscillator strengths for calculated valence states (red). Positions of $^1A_2$ states are identified by use of an arbitrary f(r) = 10^{-4}. A logarithmic plot of the calculated oscillator strengths, which emphasizes the variation in f(r) is shown in the supplementary material.[32]

FIGURE 5 The low-energyregionofthePESof*PhI*,containingthefourlowest IEs, which is relevant to the current VUV spectral analysis.

FIGURE 6 Super-position of the calculated FC profiles of the 1^1B_1 and 1^1B_2 states on the experimental band A absorption of *PhI*. The intensity of the 1^1B_1 profile has been increased by a factor of 20 for illustration purposes. A ladder generated from the vibrational modes and frequencies observed for band B is shown above the experimental

spectrum with the origin aligned with the first identifiable band in the spectrum at 4.6 eV.

FIGURE 7 Super-position of the calculated FC profile of the 1^1A1 state on the experimental band B absorption of *PhI*. The origin of the calculated FC profile has been increased by 0.408 eV to superimpose the experimental band. The fundamental vibrational bands are labelled.

FIGURE 8 The lowest Rydberg state; there is a close correlation between the observed (black trace) and calculated (red trace) envelopes, but the long tail shows minor differences from the PES band.

FIGURE 9 Low-energy region of the raw (black trace) and "background subtracted" (red trace) VUV photoabsorption spectrum of *PhI*, (a). The latter is generated by subtraction of a set of local Gaussian peaks to generate a flat baseline enabling the Rydberg state structure to be seen more clearly and has been multiplied by a factor of 5. The ladders mark the observed Rydberg series converging on IE1 which is indicated by an arrow. High-energy region of the raw (black trace) and "background subtracted" (lower red trace) spectrum, (b); the "background subtracted" spectrum multiplied by a factor of 25 is shown in the upper red trace.

FIGURE 10 Expansions of parts of the "background subtracted" VUV absorption spectrum of *PhI*. All Rydberg states have X^2B1 ionic cores unless stated otherwise. The ladders indicate $\nu 11$ progressions starting at $v = 0$.

FIGURE 11 Expansions of parts of the "background subtracted" VUV absorption spectrum of *PhI*. All Rydberg states have X^2B1 ionic cores unless stated otherwise. The ladders indicate $\nu 11$ progressions starting at $v = 0$. For $n > 6$, $(n + 1)$s-, nd-, and nf-Rydberg states are unresolved. The arrow in (b) indicates IE1 at 70 638 cm^{-1}.

FIGURE 12 Expansion of part of the "background subtracted" VUV absorption spectrum of *PhI*. All Rydberg states have C^2B1 ionic cores unless stated otherwise. For n>4, (n+1)s- and nd-states are unresolved. The arrows indicate IE1-4.

Figures

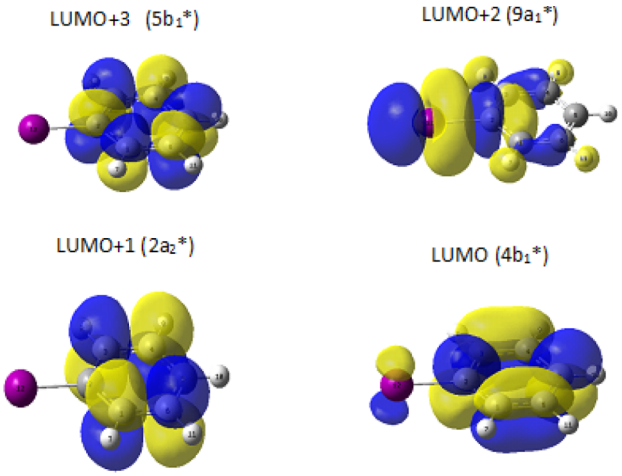

Figure 1(b)

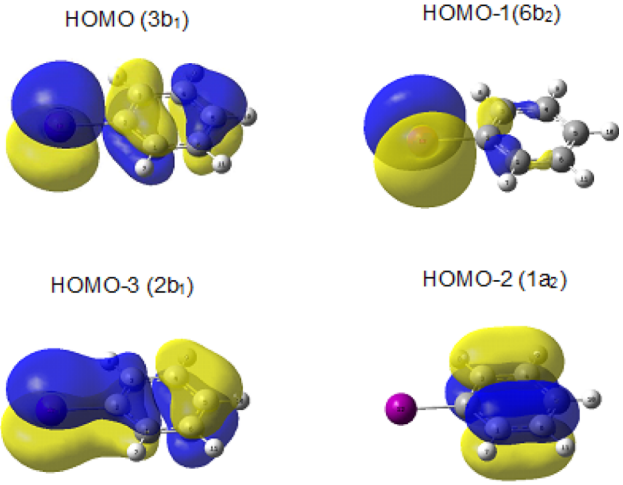

Figure 1(a)

FIGURE 1

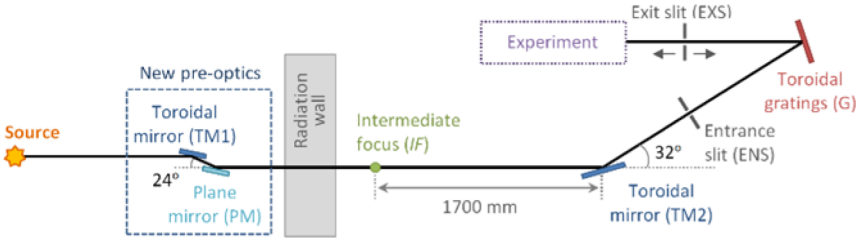

FIGURE 2

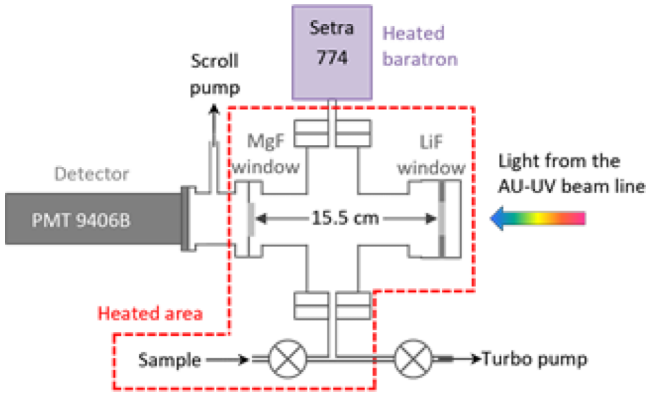

FIGURE 3

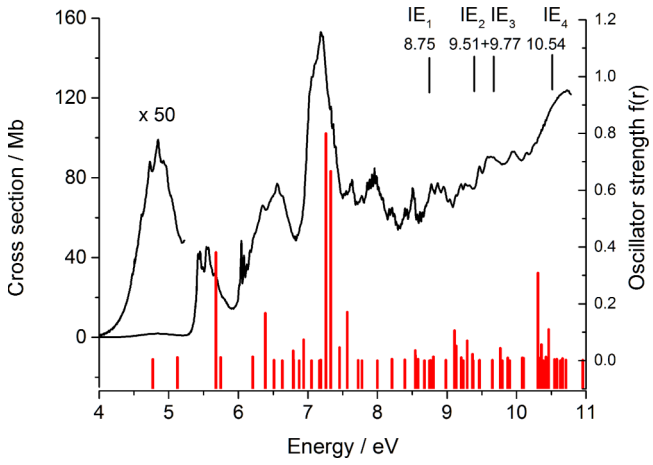

FIGURE 4

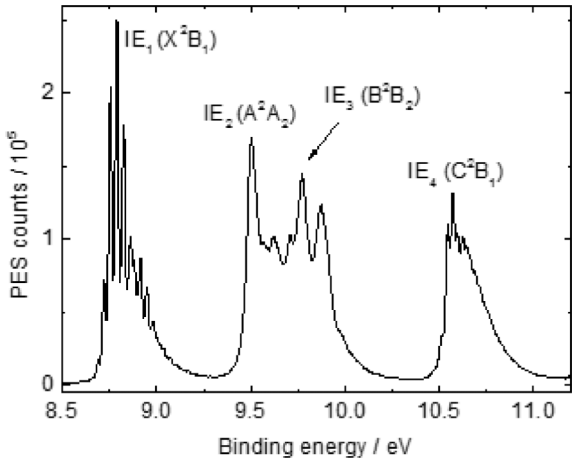

FIGURE 5

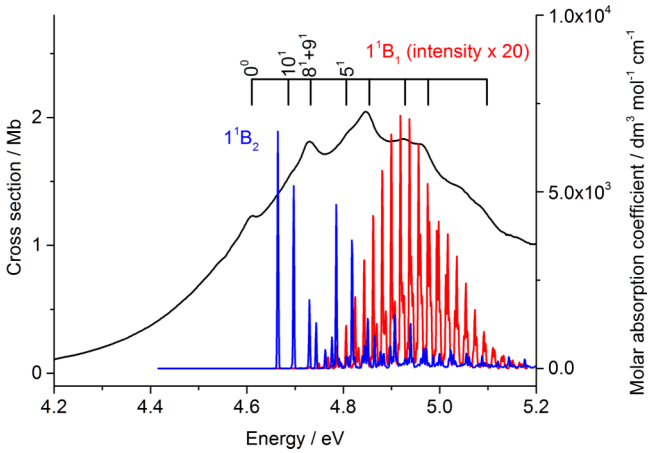

FIGURE 6

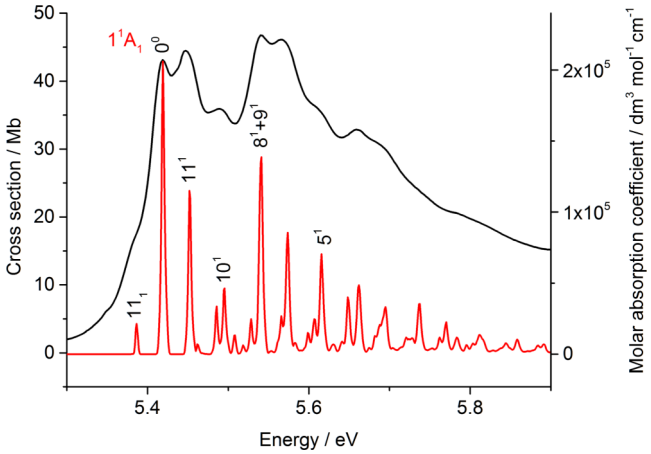

FIGURE 7

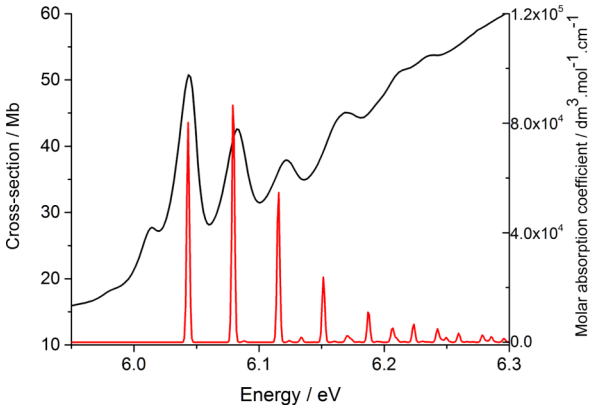

FIGURE 8

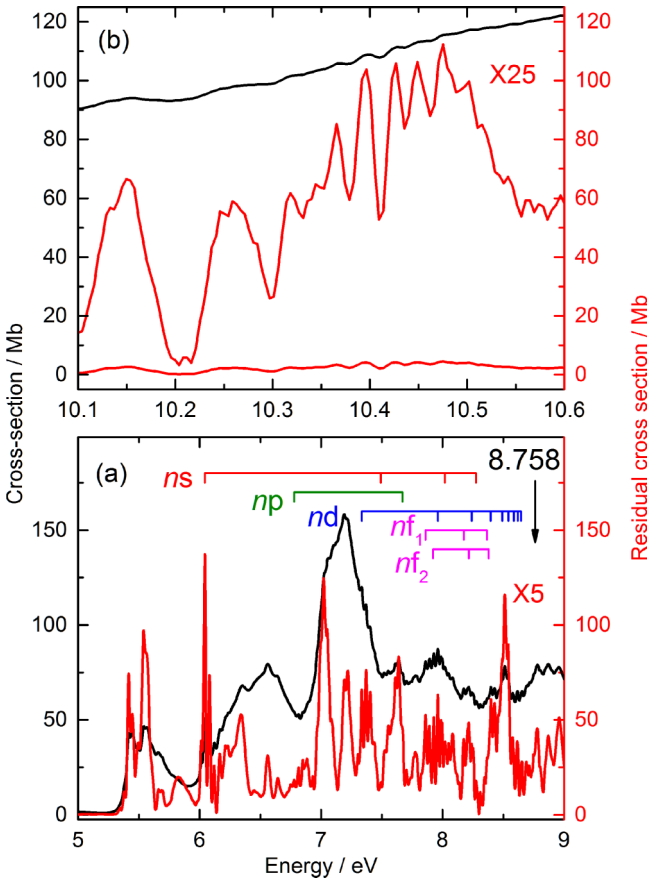

FIGURE 9

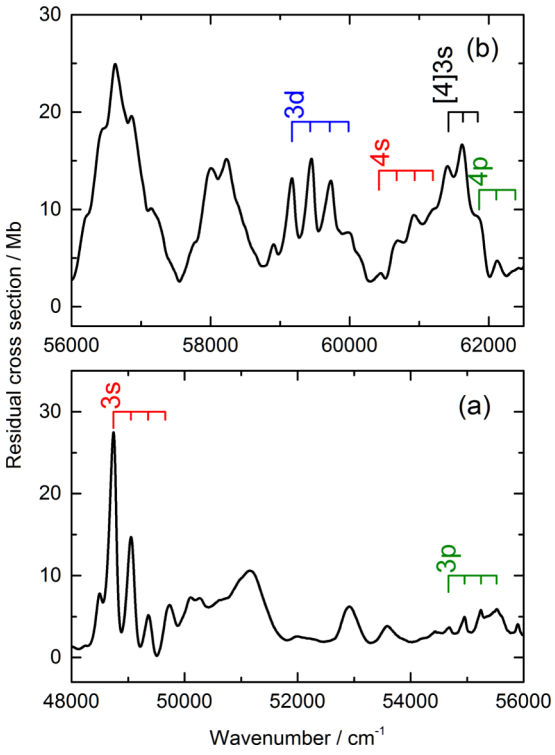

FIGURE 10

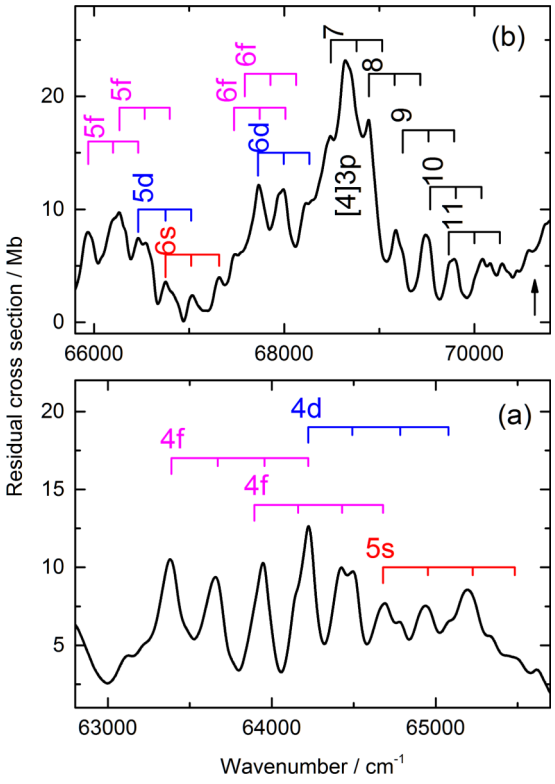

FIGURE 11

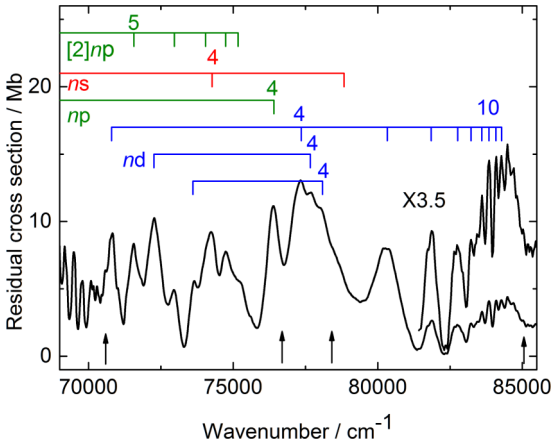

FIGURE 12

Tables

TABLE I. Experimental adiabatic IEs of *PhI* used in the Rydberg state assignments.

Expt. IE/eV (cm^{-1})	Leading term vacancy	State symmetry
8.758 (70 638)	$3b_1^{-1}$	X^2B_1
9.505 (76 663)	$1a_2^{-1}$	A^2A_2
9.776 (78 848)	$6b_2^{-1}$	B^2B_2
10.543 (85 035)	$2b_1^{-1}$	C^2B_1

TABLE II. Calculated adiabatic (TDDFT) and vertical (MRDCI) excitation energies, oscillator strengths, and spectral assignments of some valence states of *PhI*.

AEE/eV	Oscillator strength f(r)	VEE/eV	Oscillator strength f(r)	Symmetry	Leading terms
4.416	0.0011	5.088	0.0108	$^1B_1$	$4b_1a_1^*$
4.664	0.0001	4.770	0.0047	$^1B_2$	$6b_2a_1^*$
4.272	0.0000	6.631	0.0000	$^1A_2$	$2a_2a_1^*$
5.195	0.0009	6.787	0.0348	$^1B_1$	$3b_1a_1^*$
5.658	0.2089	5.677	0.3807	$^1A_1$	$4b_1b_1^*$
6.219	0.0002	6.938	0.0727	$^1B_2$	$6b_2a_1^*$
7.322	0.9726	7.258	0.7994	$^1A_1$	$2a_2a_2^* + 4b_1b_1^*$
7.522	0.5810	7.329	0.6663	$^1B_2$	$4b_1a_2$

TABLE III. The AEE, their vibrational energies, vibrational assignments, and intensities determined for several low-lying excitations, using the TDDFT method.

1^1B_1			1^1A_1		
	Intensity/			Intensity/	
Energy/cm^{-1}	$dm^3\,mol^{-1}\,cm^{-1}$	Assignment	Energy/cm^{-1}	$dm^3\,mol^{-1}\,cm^{-1}$	Assignment
2276	65	11^{15}	266	207 200	11^1
2428	101	11^{16}	532	45 980	11^2
2580	144	11^{17}	612	90 200	10^1
2732	186	11^{18}	878	33 610	$10^1 11^1$
2883	220	11^{19}	970	124 300	9^1
2942	47	$9^2 11^{19}$	984	217 500	8^1
3035	237	11^{20}	1184	35 440	6^1
3094	51	$9^2 11^{20}$	1236	58 060	$9^1 11^1$
3187	233	11^{21}	1250	106 400	$8^1 11^1$
3246	50	$9^2 11^{21}$	1581	78 870	5^1
3339	210	11^{22}	1582	21 750	$9^1 10^1$
3490	172	11^{23}	1597	41 310	$8^1 10^1$
3642	127	11^{24}	1847	34 100	$5^1 11^1$
3794	86	11^{25}	1954	59 710	$8^1 9^1$
			1968	50 660	8^2
			2220	28 650	$8^1 9^1 11^1$
			2565	35 430	$5^1 8^1$

1^1B_2			$^1B_1$ 3s-Rydberg		
	Intensity/			Intensity/	
Energy/cm^{-1}	$dm^3\,mol^{-1}\,cm^{-1}$	Assignment	Energy/cm^{-1}	$dm^3\,mol^{-1}\,cm^{-1}$	Assignment
265	5163	11^1	291	86 480	11^1
529	1937	11^2	582	43 400	11^2
641	1287	10^1	873	23 720	11^3
905	881	$10^1 11^1$	1162	3 834	7^1
978	4632	8^1	1164	7 131	11^4

1243	3625	$8^1 11^1$	1316	3	404	6^1
1459	626	5^1	1453	3	797	$7^1 11^1$
1507	1383	$8^1 11^2$	1607	3	004	$6^1 11^1$
1619	912	$8^1 10^1$				
1883	638	$8^1 10^1 11^1$				
1956	1389	8^2				
2221	1108	$8^2 11^1$				

2^1B_2						
Intensity/						
Energy/cm^{-1}	$dm^3\,mol^{-1}\,cm^{-1}$	Assignment				
6208	68	11^{45}				
6345	104	11^{46}				
6483	105	11^{47}				
6621	97	11^{48}				
6759	81	11^{49}				
6897	104	11^{50}				
7035	90	11^{51}				
7173	75	11^{52}				
7311	64	11^{53}				

TABLE IV. Transition energies, T_E (cm^{-1}) and n* values of the origin bands of the Rydberg states of *PhI* converging on various states of the ion observed in the VUV absorption spectrum.

X^2B_1 n* values calculated using IE_1 of 70 638 cm^{-1}.[49]										
	ns		np		nd		nf_1		nf_2	
n	T_E/cm^{-1}	n*	T_E/cm^{-1}	n*	T_E/cm^{-1}	n*	T_E/cm^{-1}	n*	T_E/cm^{-1}	n*
3	48 742	2.24	54 671	2.62	59 168	3.09				
4	60 419	3.28	61 858	3.54	64 222	4.14	63 387	3.89	63 893	4.03
5	64 678	4.29			66 461	5.13	65 937	4.83	66 265	5.01
6	66 751	5.31			67 723	6.14	67 472	5.89	67 585	6.00
7					68 489	7.15				
8					68 890	7.92				
9					69 247	8.88				
10					69 536	9.98				
11					69 730	11.00				

A^2A_2 n* values calculated using IE_2 of 76 663 cm^{-1}.							
	np						
n	T_E/cm^{-1}	n*					
5	71 551	4.64					
6	72 961	5.45					
7	74 044	6.48					
8	74 734	7.57					
9	75 155	8.55					

C^2B_1 n* values calculated using IE_4 of 85 035 cm^{-1}.										
	ns		np		nd_1		nd_1		nd_2	
n	T_E/cm^{-1}	n*	T_E/cm^{-1}	n*	T_E/cm^{-1}	n*	T_E/cm^{-1}	n*	T_E/cm^{-1}	n*
3	61 402	2.15	68 708	2.59	70 790	2.78	72 276	2.93	73 633	3.10
4	74 234	3.19	76 389	3.56	77 364	3.78	77 694	3.87	78 058	3.97
5	78 835	4.21			80 284	4.87				

6					81 828	5.85				
7					82 742	6.92				
8					83 222	7.78				
9					83 606	8.76				
10					83 852	9.63				
11					84 099	10.83				
12					84 276	12.02				